X-ray absorption spectroscopy study of the Ni K edge in magnetron-sputtered nickel oxide thin films

1997 J. Phys.: Condens. Matter 9 6979

(http://iopscience.iop.org/0953-8984/9/32/019)

J. Phys.: Condens. Matter **9** (1997) 6979–6993. Printed in the UK PII: S0953-8984(97)81016-8

X-ray absorption spectroscopy study of the Ni K edge in magnetron-sputtered nickel oxide thin films

A Kuzmin, J Purans and A Rodionov

Institute of Solid State Physics, 8 Kengaraga Street, LV-1063 Riga, Latvia

Received 16 January 1997, in final form 6 May 1997

Abstract. Nickel oxide, NiO_x, thin films were studied by means of x-ray absorption spectroscopy at the Ni K edge. Thin films were prepared by reactive dc magnetron sputtering of a nickel target in an atmosphere that was an Ar–O_2 mixture. The results of the EXAFS analysis show that the thin films have nanocrystalline structure, which can be described within the non-reconstructed grain-boundary model. Average grain sizes of 21 ± 3 Å and 34 ± 5 Å were obtained for thin films deposited in sputter atmospheres with oxygen contents of 30% and 100%, respectively. The nanocrystalline structure of the thin films results in a reduction in the number of atomic neighbours in the crystal lattice coordination shells beyond the first one. Also, increases of the structural disorder and of the intragrain lattice parameter relative to those for crystalline NiO (c-NiO) were detected for the thin films. In the XANES region, the intensity of the pre-edge peak, attributed to the dipole-allowed transitions $|1s3d^{8+i}\underline{L}^i\rangle \rightarrow |\underline{1s}3d^{8+i}\underline{L}^{i-1}\rangle$, $i = 1, 2$ (where $\underline{L}$ denotes an O 2p hole and $\underline{1s}$ stands for a Ni 1s core hole), was found to be smaller in the thin films than in c-NiO. This result was interpreted within the Zaanen–Sawatzky–Allen model as being due to an increase of the oxygen–nickel charge-transfer energy which is accompanied by a reduction of the extent of the $3d^{8+i}\underline{L}^i$ $(i = 1, 2)$ ground-state configuration. The findings on the local atomic and electronic structures suggest that, compared to that for c-NiO, the ionicity of the nickel–oxygen bonding increases significantly in the thin films.

1. Introduction

Nickel oxide thin films are important materials, with possible application in electrochromic coatings [1] and transparent electrodes [2]. Their chemical composition can be represented as NiO_xH_y, but, for simplicity, it is usually referred to as NiO_x. From the viewpoint of the electrochromic properties, reviewed recently by Granqvist [3], NiO_x films exhibit anodic coloration associated with proton extraction [1] and formation of Ni^{3+} colour centres [4]. According to their electrical properties, NiO_x thin films are p-type semiconductors whose resistivity can be lowered by an increase of the hole concentration: this can be achieved by an increase of the number of native defects, such as nickel vacancies and/or interstitial oxygen, or by doping with monovalent ions, such as lithium [5].

Thin films of nickel oxide can be produced by different methods, such as evaporation, sputter deposition, and electrochemical and chemical techniques [3]. Among these, magnetron sputtering [1, 2, 4] is a particularly attractive method for large-area high-rate thin-film manufacture. The electrical and optical properties of NiO_x films prepared by reactive magnetron sputtering depend primarily on the O_2 content in the $Ar + O_2$ sputter atmosphere [2]. As-deposited NiO_x films have a grey/brown colour, which suggests the presence of not only Ni^{2+} but also some Ni^{3+} ions [2]. In spite of a large number of studies having been published during the last few years on electrochromism in NiO_x (see the review

0953-8984/97/326979+15$19.50

by Granqvist [3]), the physical mechanism of the optical absorption in Ni-oxide-based films is still not clear [6, 7]. Also, full clarity regarding the structure of NiO_x thin films has not been achieved [3].

The correlation between the properties and atomic structure of nickel oxide thin films was studied previously by means of electron [8–10] and x-ray [4, 11–15] diffraction, and x-ray absorption spectroscopy (XAS) [16, 17]. Electron diffraction has shown that the structure of the films is dominated by a fcc NiO-like phase [8–10]. More detailed information was obtained by means of x-ray diffraction (XRD); however, one should note that the films exhibit only weak diffraction peaks in the x-ray diffraction patterns. A number of XRD studies [11–13, 15] indicated a NiO-type structure, whereas some studies [4, 14] showed the presence of a disordered Ni_2O_3 phase which transforms to NiO when the thin film is annealed at temperatures above 300 °C [14]. The minority phase of Ni_3O_4 ($NiO{\cdot}Ni_2O_3$) was also observed by x-ray photoelectron spectroscopy (XPS) in films made by dc and rf sputtering in an $Ar + O_2$ sputter atmosphere [8, 13, 15]. The lattice parameter of the NiO_x films was found to be 4.22 Å for samples annealed at 120 °C, and it decreased slightly to the bulk value of 4.17 Å after annealing at 400 °C [15]. Thus diffraction studies suggest that NiO_x films are composed of small crystalline grains with a structure close to that of crystalline NiO (c-NiO). A fine-grained crystallinity of nickel oxide thin films was also supported by transmission electron microscopy (TEM) [8, 9, 18]: the presence of grains with average sizes of 15 to 170 Å within the thin-film structure was reported.

Information which is complementary to that obtained from diffraction techniques can be obtained by XAS. In contrast to diffraction, XAS is a local and site-sensitive probe providing information about both the electronic and atomic structures around the absorbing centre.

The first application of XAS to the study of the local environment around nickel ions in NiO_x thin films was performed in [16]. The difference between the Ni K-edge x-ray absorption spectra of c-NiO and NiO_x thin film was interpreted on the basis of a microcrystalline model of the thin-film structure with a significant degree of disorder present within it [16]. Similar conclusions were obtained in our recent work [17]. However, accurate information on the local environment around nickel ions has still not been established.

In this paper, we present an accurate x-ray absorption spectroscopy study of the local environment around nickel ions in NiO_x thin films, prepared by reactive dc magnetron sputtering. The analysis of the Ni K-edge x-ray absorption spectra in thin films is performed in comparison with the case of crystalline c-NiO. The results obtained on the local electronic structure around nickel ions are interpreted within the Zaanen–Sawatzky–Allen framework [19]. The information on the atomic structure is described in terms of the non-reconstructed grain-boundary model of nanocrystals [20]. As a result, the correlations between the atomic and electronic structures of the thin films are established, and a number of characteristic parameters are determined.

2. Experimental details

Nickel oxide thin films were prepared by reactive magnetron sputtering in a plasma-focusing DC magnetic field at a discharge power of 100 W. A metallic nickel (purity 99.7%) plate of dimensions 140 × 100 mm was used as the target. Before sputtering, the chamber was evacuated to 3×10^{-5} Torr. A gas mixture of argon and oxygen ($Ar + O_2$) was used as the sputter atmosphere; the oxygen content in the sputter gas was 100% for sample No 1 and 30% for sample No 2. The sputter deposition was performed for one hour at a total gas pressure 0.06 Torr for sample No 1 and 0.05 Torr for sample No 2. The polyimide

film substrates were mounted ∼8 cm above the target, and were not intentionally heated; however, their temperatures reached about 100 °C during the sputter deposition. Pre-sputtering took place for ∼15 min prior to the thin-film deposition. All of the as-deposited films thus obtained were coloured.

A commercial crystalline nickel oxide (c-NiO) powder was used as a reference; its single-phase structure was confirmed by powder XRD measurements. For x-ray absorption measurements, c-NiO powder was finely ground and homogeneously deposited on a polytetrafluoroethylene membrane by a sonication technique.

X-ray absorption spectra were recorded in transmission mode at the PWA-BX1 wiggler beamline using synchrotron radiation from the ADONE storage ring [17]. The storage ring ADONE operated at the energy 1.2 GeV and a maximum stored current of 40 mA. A standard transmission scheme with a Si(111) ($2d = 6.271$ Å) channel-cut crystal monochromator and two ion chambers containing krypton gas was used. The spectra were measured at room temperature in the energy range up to ∼750 eV above the Ni K edge, with energy steps of 1 eV in the near-edge region and 2 eV above the edge. The experimental energy resolution was estimated to be about 1 eV. The sample thickness x resulted in an absorption edge jump $\Delta\mu x$ equal to ∼0.75 for c-NiO and ∼0.25 for the thin films (μ is the absorption coefficient).

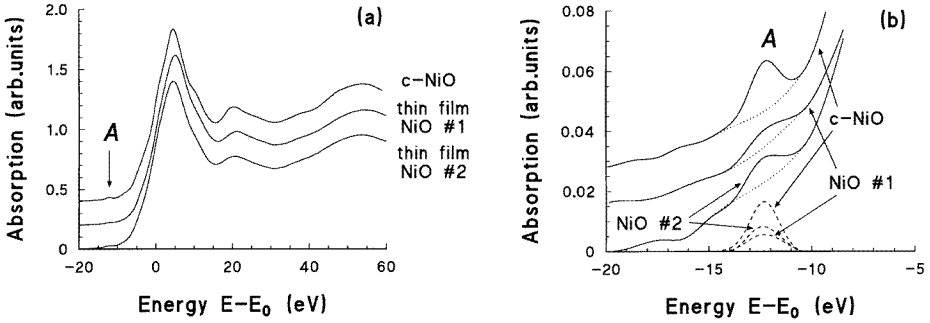

Figure 1. (a) Normalized experimental XANES spectra of the Ni K edge in c-NiO and the thin films No 1 and No 2. The position of the pre-edge peak A is shown. The energy origin E_0 was chosen as in [21]. (b) An expanded view of the pre-edge part of the Ni K-edge XANES (solid lines). The dotted lines are background approximations determined by a cubic spline fit to the data on either side of the pre-edge peak A. The peak A, singled out by subtracting the background contribution from the experimental XANES signal, is shown by a dashed line. Note that its intensity is smaller in the thin films than in c-NiO.

3. Data analysis and results

3.1. Nickel K-edge XANES

The region of the x-ray absorption near-edge structure (XANES) in c-NiO and the thin films is shown in figure 1(a). As in our previous study of $Ni_cMg_{1-c}O$ solid solutions [21], the E_0-position was set at the maximum of the first derivative of the absorption coefficient in c-NiO, and was fixed for all of the spectra at the same energy. The shape of the XANES is rather similar for all of the samples, except that it is slightly broadened in the thin films. Also the pre-edge peak A (figures 1(a), 1(b)) is present in all of the spectra. Its position (about 12 eV below E_0) and the full width at half-maximum (FWHM) (∼1.5 eV) for c-NiO

are close to those for the thin films; however, its intensity I_A is smaller for the thin films (I_A(No 1) = 0.012 and I_A(No 2) = 0.015) than for c-NiO (I_A = 0.029). The origin of the peak A and of the difference in its intensity will be discussed in detail in section 4.

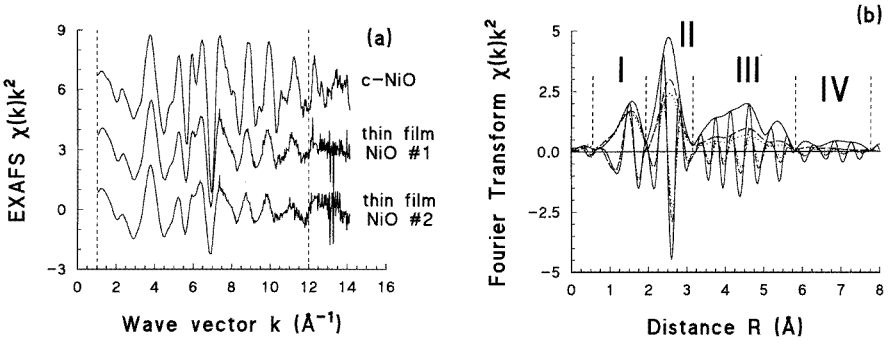

Figure 2. (a) Experimental EXAFS $\chi(k)k^2$ spectra of the Ni K edge for c-NiO and the thin films. In spite of the general similarity of the shapes of the EXAFS signals, a larger amplitude damping and a slightly higher frequency of the EXAFS signal are observed for the thin films. The range (1–12 Å^{-1}) of the Fourier transform (FT) is shown by two dashed lines. (b) FTs of the EXAFS spectra shown in (a): solid line: c-NiO; dashed line: thin film No 1; and dotted line: thin film No 2. Both the magnitude and the imaginary part of the FT are presented. The four intervals (I, II, III, and IV) of the back-FTs are indicated by vertical dashed lines.

3.2. Nickel K-edge EXAFS

The x-ray absorption spectra were treated using the 'EDA' software package, following the standard procedure [22]. The experimental extended x-ray absorption fine-structure (EXAFS) spectra $\chi(k)k^2$ of the thin films and c-NiO are shown in figure 2(a). The FTs (figure 2(b)) of the EXAFS signals, multiplied by a Kaiser–Bessel (KB) window with a parameter $A = 1.5$ [22], were calculated over the range from 1 to 12 Å^{-1}, to exclude the high-energy part ($k > 12$ Å^{-1}), strongly distorted by the presence of glitches (see figure 2(a)). Note that since no phase correction was included in the calculation of the FTs, the positions of the peaks in figure 2(b) differ by ∼0.45 Å from their true crystallographic values. The EXAFS signals corresponding to the four regions I, II, III, and IV, separated by vertical dashed lines in figure 2(b), were singled out by the back-FTs, and are shown in figure 3 by solid lines. We should perhaps point out that a difference between the EXAFS signals or their FTs in the thin films and c-NiO is typical of the behaviour of the nanocrystalline materials: the main changes occurring in the thin films are related to the reduction in the magnitudes of the FT peaks with increasing interatomic spacing, while the positions and widths of the peaks vary slightly. It should be pointed out that since the FT of the EXAFS signal is not a radial distribution function, the change of the FT-peak magnitude cannot be used as an estimate of the coordination number variation. To determine structural parameters, a precise analysis of the EXAFS signal, using one of the known approaches [23], should be performed.

The EXAFS oscillation from a group of atoms is described by a sinusoidal-like signal modulated by the photoelectron scattering amplitude function. Therefore, when the atoms constituting two groups are located in the Periodic Table far away one from another, the shapes of their EXAFS signals are very different, and, in principle, can be used for the identification of the origin of the EXAFS signals. In the particular case of oxygen and

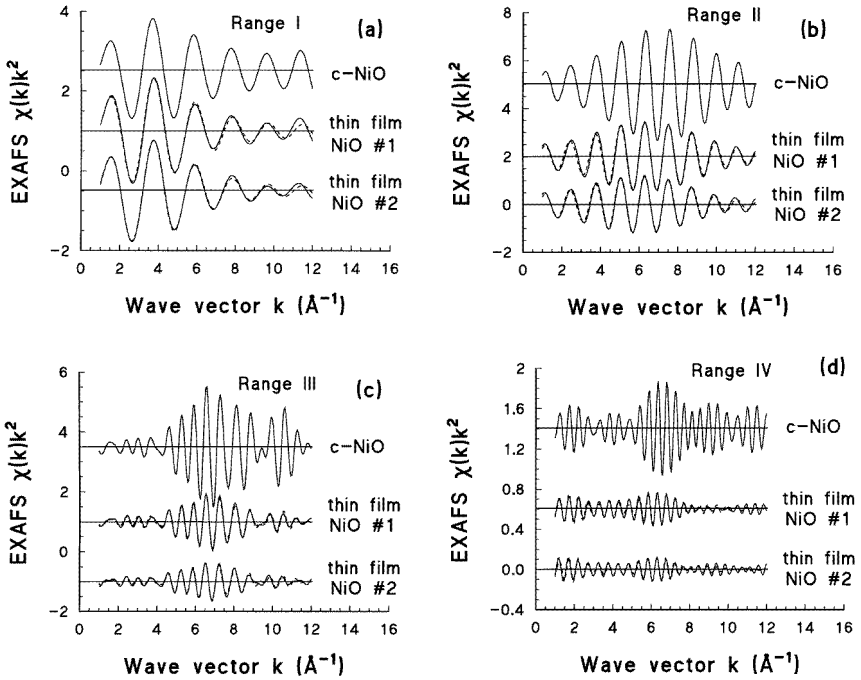

Figure 3. The experimental (solid lines) and calculated (dashed lines) EXAFS $\chi(k)k^2$ signals of c-NiO and nickel oxide thin films. The panels (a), (b), (c), and (d) correspond, respectively, to the four intervals I, II, III, and IV of the FTs indicated in figure 2.

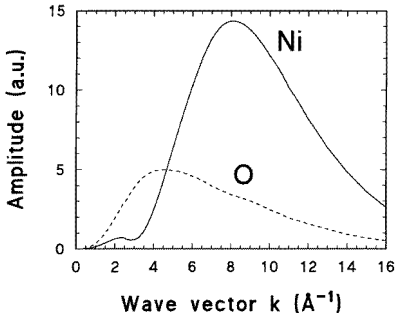

Figure 4. Theoretical backscattering amplitude functions $f(k)$ of oxygen (dashed line) and nickel (solid line) atoms multiplied by the term $\exp(-2\sigma^2k^2)k^2$ (with $\sigma^2 = 0.005$ Å^2), for direct comparison with the experimental signals shown in figure 3. Note that the amplitude maxima are located at $\sim$4 Å^{-1} for O and $\sim$8 Å^{-1} for Ni. For details of the calculation, see [21].

nickel atoms, which are separated in the Periodic Table by twenty elements, the maxima of the respective scattering amplitudes are shifted relative to one another by $\sim$4 Å^{-1} (figure 4); due to this, the oxygen atoms contribute mainly at low wave-vector values, while the nickel atoms contribute in the middle part of the usual EXAFS range. This difference will be used further to identify the types of atom which produce the main contribution to the EXAFS signals from the regions I, II, III, and IV, shown in figure 2(b).

For crystalline NiO (c-NiO), which has the rock-salt structure with the nickel ions forming a face-centred-cubic (fcc) lattice, the regions I, II, III, and IV can be attributed to the following groups of nickel and oxygen atoms. The first region, I (0.6–1.9 Å), corresponds to the first coordination shell, composed of six oxygen atoms. The second region, II (1.9–3.2 Å), is related mainly to the second shell consisting of 12 nickel atoms [21]. The third, III (3.2–5.8 Å), and the fourth, IV (5.8–7.8 Å), regions correspond to the outer shells, among which the ones containing nickel ions produce the main contribution to the EXAFS signal. This conclusion is supported by the shape of the EXAFS amplitude function (figures 3(c), 3(d)), which is similar to the scattering amplitude function of the nickel atoms, with a maximum at $\sim$8 Å^{-1} (figure 4). The result obtained does not mean that the oxygen atoms of the outer shells do not contribute to the Ni K-edge x-ray absorption spectrum of c-NiO at all, but that their contribution is larger at low energies, and, thus, compared to the contribution of the nickel atoms, is more important in the XANES region [24] than in the EXAFS region. This result can also be explained in part by the large difference of the oxygen and nickel atomic masses, which leads to a higher value of the vibrational amplitude of the lighter oxygen atoms, and as a result to a larger thermal damping of the Ni–O EXAFS signals (with respect to the Ni–Ni EXAFS signals) at high energies.

A comparison of the experimental EXAFS signals for c-NiO and the thin films reveals a substantial similarity of their shapes, both in k-space (figure 2(a)) and in R-space (figure 2(b)). In fact, the main difference between crystal and thin-film spectra is the larger amplitude damping in the latter, while the frequencies of their EXAFS oscillations remain very close. These findings also apply to the EXAFS signals (figure 3) from each of the four ranges indicated in figure 2(b). The qualitative behaviour of the EXAFS oscillations for nickel oxide thin films seems to be in agreement with their nanocrystalline microstructure observed via TEM measurements [8, 9, 18] and supported by previous EXAFS studies [16, 17]. It is assumed that the structure of such materials is composed of randomly oriented nanosized crystallites, whose internal structure coincides with or is close to that of the parent crystal. The random relative orientation of crystallites leads to the loss of atom–atom correlations at the crystallite boundaries [20], so it is just the internal ordered region of the crystallites that is responsible for the form of the pair atomic distribution function, while the presence of boundaries results only in the modification of its amplitude (i.e. in a reduction of the coordination numbers). Therefore, it seems possible to use the EXAFS signal of a crystalline compound as a reference for its nanocrystalline counterpart. As long as the structural information included in the EXAFS of the nanocrystal can be assumed to be related just to the ordered regions, whose structure is similar to that of the reference compound, one can rely on the amplitude and phase transferability of the EXAFS signals. In our case, to describe the nanocrystalline structure of NiO_x thin films quantitatively, a comparative approach, with c-NiO crystal taken as the reference compound, was used.

The EXAFS signals of the thin films were fitted within each of the four ranges (figure 2(b)) using a simple model

$$\chi(k) = A_r \exp(-2\,\Delta\sigma^2 k^2) F^{\mathrm{c-NiO}}(k) \sin(2k\,\Delta R + \Phi^{\mathrm{c-NiO}}(k)) \qquad (1)$$

where $k = \sqrt{(2m_e/\hbar^2)(E - E_0)}$ is the photoelectron wave vector; $A_r = N_r S_{0r}^2$ is the relative amplitude, equal to the product of the relative coordination number $N_r = N/N^{\mathrm{c-NiO}}$ and the relative amplitude reduction factor $S_{0r}^2 = S_0^2/(S_0^2)^{\mathrm{c-NiO}}$; $\Delta R = R - R^{\mathrm{c-NiO}}$ is a difference of interatomic distances; and $\Delta\sigma^2 = \sigma^2 - (\sigma^{\mathrm{c-NiO}})^2$ is the relative EXAFS Debye–Waller factor. Note that σ^2 ($=\sigma_{\mathrm{th}}^2 + \sigma_{\mathrm{st}}^2$) has the meaning of a *mean square relative displacement* (MSRD), and includes both thermal σ_{th}^2 and static σ_{st}^2 disorder. The factor S_0^2 corresponds to the overlap between the initial- and the final-state wave functions of the

$Z-1$ passive electrons which are excited along with the photoelectron [25]. It is considered to be dependent only on the central atom (absorber) [25]; therefore the values of S_0^2 are assumed to be equal for c-NiO and the thin films: $(S_0^2)^{\text{thin film}} = (S_0^2)^{\text{c-NiO}}$, so $S_{0r}^2 = 1$ and $N_r = A_r$.

The functions $F^{\text{c-NiO}}(k)$ and $\Phi^{\text{c-NiO}}(k)$ used in equation (1)

$$F^{\text{c-NiO}}(k) = \frac{N^{\text{c-NiO}}(S_0^2)^{\text{c-NiO}}}{k(R^{\text{c-NiO}})^2} \exp(-2(\sigma^{\text{c-NiO}})^2 k^2) f(k) \tag{2}$$

$$\Phi^{\text{c-NiO}}(k) = 2kR^{\text{c-NiO}} + \phi(k) \tag{3}$$

are the amplitude and the phase of the EXAFS signal for c-NiO obtained by the back-FT procedure within the range of interest (here $f(k)$ and $\phi(k)$ denote the total scattering amplitude and phase-shift functions, respectively). Note that in the present transcription of equation (2), the following simplification was made: $(R^{\text{c-NiO}} + \Delta R)^2 \approx (R^{\text{c-NiO}})^2$. Since in our case $\Delta R \ll R^{\text{c-NiO}}$, the approximation is valid; this is also supported by an excellent coincidence of the results obtained in the test calculation using the approximate and exact forms of equation (2).

Table 1. Best-fit *relative* values of the average coordination numbers N_r (± 0.15), distances ΔR (± 0.01 Å), and MSRDs $\Delta\sigma^2$ (± 0.001 Å^2) for nickel oxide thin films (see equation (1) for details).

Peak number	Thin film No 1			Thin film No 2		
	N_r	ΔR (Å)	$\Delta\sigma^2$ (Å^2)	N_r	ΔR (Å)	$\Delta\sigma^2$ (Å^2)
I	1.12	−0.02	0.005	1.13	−0.02	0.006
II	0.86	0.01	0.003	0.83	0.02	0.005
III	0.67	0.03	0.004	0.52	0.04	0.005
IV	0.69	0.02	0.008	0.55	0.06	0.009

From the fit using equation (1), a set of three parameters, A_r, ΔR, and $\Delta\sigma^2$ (see table 1), were obtained for each of the four ranges (figure 2(b)). (For comparison, the maximum number of fitting parameters allowed by the Nyquist criterion [26] is about 12, 9, 20, and 14 for the ranges I, II, III, and IV, respectively.) The fitted EXAFS signals are shown in figure 3 by dashed lines. In spite of great simplicity of the model utilized, the agreement between the experimental and calculated EXAFS is surprisingly good; the discrepancy observed at the beginning and at the end of the k-space range can be attributed to the influence of the Fourier filtering procedure and to the significant level of noise present in the original EXAFS data for the thin films with k above ~ 10 Å^{-1} (figure 2(a)).

Table 2. Calculated parameters of the reconstructed grain-boundary model for nickel oxide thin films (see section 3.3 for details).

Sample	x_L	α_{GB} (Å^{-1})	$\langle D\rangle_{\text{area}}$ (Å)	t (Å)
Thin film No 1	0.96 ± 0.15	0.089 ± 0.014	34 ± 5	0.5 ± 0.2
Thin film No 2	0.99 ± 0.15	0.142 ± 0.022	21 ± 3	0.1 ± 0.03

3.3. The reconstructed grain-boundary model [20]

The parameters in table 1, obtained from the analysis of the EXAFS spectra, can be related to the structure of nickel oxide thin films using the *reconstructed grain-boundary* (RGB) model, suggested recently in [20] for the description of the structure of nanocrystalline solids. Within the RGB model, it is assumed that a solid consists of crystalline-like grains, having the same arrangements of atoms as in the extended lattice, and oriented randomly with respect to one another, and a grain-boundary (GB) region, comprising all of the atoms which are situated in the grain boundaries between the crystallites and are displaced from their lattice positions to new, non-lattice equilibrium positions [20]. Note that in the case of the grain-boundary atoms remaining at their lattice positions, one deals with the *non-reconstructed grain-boundary* (NRGB) model [20, 27].

According to equation (12) in [20], the short-range order (SRO) component of the total pair atomic distribution function within the RGB model is given by

$$\rho^{\mathrm{SRO}}(r) = x_L H(r) \rho^V(r) \tag{4}$$

where x_L denotes the ratio of the number of atoms on crystal lattice sites to the total number of atoms in the solid, $H(r)$ is the intragrain correlation function [20, 28], and $\rho^V(r)$ is the atomic distribution function of the extended crystal lattice. $H(r)$ decreases linearly from the value unity at $r = 0$, with an initial slope proportional to the specific free surface area of the grain, α_S [20]:

$$H(r) = 1 - \frac{\alpha_S}{4} r \qquad (r \ll D) \tag{5}$$

where D is the grain size. For the grains having similar shape, α_S is proportional to the inverse of the area-weighted average grain size, $\langle D \rangle_{\mathrm{area}}$. In the particular case of spherical grains, $\alpha_S = 6\langle D \rangle_{\mathrm{area}}^{-1}$. Note that in solids, since two grains form a single grain boundary, the specific grain-boundary area is half the specific surface area: $\alpha_{\mathrm{GB}} = 3\langle D \rangle_{\mathrm{area}}^{-1}$.

The size of the grain-boundary region can be roughly estimated within the RGB model: if one assumes that the number of atoms on non-lattice positions per unit area of grain boundary is independent of the grain size, then the thickness t of a hypothetical disordered grain-boundary layer of the same density as the crystal lattice is equal to $(1 - x_L)/\alpha_{\mathrm{GB}}$ [20]. Note that the case where $t = 0$ is referred to as the *non-reconstructed grain-boundary* model [20], mentioned before.

Thus, to obtain quantitative information on the atomic SRO within the RGB model, one needs to determine the quantities x_L and α_{GB}. They can be found, supposing that $\rho^V(r)$ is known, from the experimental atomic distribution function, using equations (4) and (5): the function $x_L H(r)$ is obtained as the straight line representing the best fit to the dependence of the relative reduction in coordination number on the interatomic distance [20]. The value of $x_L H(r)$ at $r = 0$ corresponds to x_L since $H(0) = 1$, while the slope of $x_L H(r)$ allows us to determine α_{GB} [20]. The parameters determined by this method (see figure 5(a)) are presented in table 2.

4. Discussion

As has been mentioned in section 3.1, the main difference between the Ni K-edge XANES spectra for the thin films and for c-NiO lies in the intensity of the pre-edge peak A (figure 1(b)). We will give an explanation for this phenomenon within the framework of the so-called Zaanen–Sawatzky–Allen (ZSA) model [19], and will relate it to the results of the EXAFS analysis.

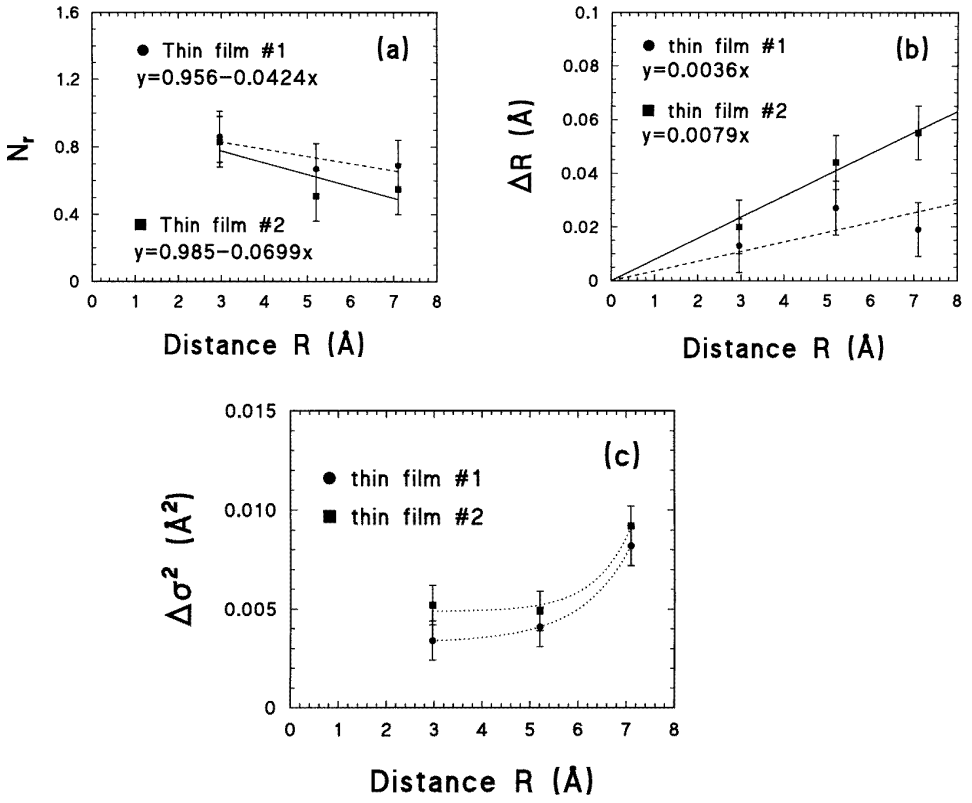

Figure 5. (a) The ratio $N_r = N_i/N_i^{\mathrm{c-NiO}}$ of the number of nickel atoms determined as being in the coordination shell i, N_i, to the ideal single-crystal value for that shell, $N_i^{\mathrm{c-NiO}}$, versus the interatomic spacing R_i. Straight lines (dashed for thin film No 1 and solid for thin film No 2) correspond to the function $x_L H(R)$ ($\equiv x_L - x_L(\alpha_S/4)R$) obtained by linear least-squares fitting to the data; the numbers given within the figures indicate the fit parameters. (b) The difference of the interatomic distances ΔR_i ($\equiv R_i - R_i^{\mathrm{c-NiO}}$) for the second, third, and fourth ranges shown in figure 2. The slope δa of the straight lines determines the expansion of the intragrain lattice parameter a in the thin films: $a = a^{\mathrm{c-NiO}}(1 + \delta a)$, where $a^{\mathrm{c-NiO}} = 4.1795$ Å [46]. For thin film No 1 (dashed line), $\delta a = 0.0036$ and $a^{\mathrm{No\ 1}} = 4.20$ Å. For thin film No 2 (solid line), $\delta a = 0.0079$ and $a^{\mathrm{No\ 2}} = 4.21$ Å. (c) The difference of the MSRDs $\Delta\sigma_i^2$ ($\equiv \sigma_i^2 - (\sigma_i^{\mathrm{c-NiO}})^2$) for the second, third, and fourth ranges indicated in figure 2. The dotted lines are only guides for the eye.

In terms of the ZSA classification [19, 29], insulating compounds can be divided into Mott–Hubbard-type ($\Delta > U$) and charge-transfer-type ($U > \Delta$) compounds according to the relative value of the d–d Coulomb correlation energy U and the ligand p-to-metal 3d charge-transfer energy Δ. Here Δ is the only parameter of the model which is strongly anion dependent: it is given roughly by the electronegativity difference $(X_{\mathrm{a}} - X_{\mathrm{c}})$ between the anion and the cation [29, 30]. Therefore, Δ increases when the anion–cation pd covalent mixing, λ_{pd}, decreases, and the bonding becomes more ionic. According to XPS and XAS studies [29, 31], crystalline nickel oxide belongs to the class of charge-transfer insulators with $\Delta = E(\mathrm{t}_{2\mathrm{g}}^6\mathrm{e}_{\mathrm{g}}^3\underline{L};\, ^3\mathrm{A}_2) - E(\mathrm{t}_{2\mathrm{g}}^6\mathrm{e}_{\mathrm{g}}^2,\, ^3\mathrm{A}_2) \sim 4.6$ eV and $U \sim 5$ eV ($\Delta = 4.5$ eV and $U \sim 7.5$ eV were obtained in [33]). Within a cluster-type configuration-interaction model

[29, 33], the ground state (GS) of NiO is described as

$$\Psi_{GS} = a_0|3d^8\rangle + a_1|3d^9\underline{L}\rangle + a_2|3d^{10}\underline{L}^2\rangle \tag{6}$$

where $\underline{L}$ stands for an oxygen 2p hole. The proportions a_i ($i = 0, 1, 2$) of the $|3d^{8+i}\underline{L}^i\rangle$ configurations are 0.73, 0.21, and 0.06 (see table II in [29]), respectively, so only the first two of them are significant in the ground state.

In the case of the Ni K-edge absorption, the transition of the 1s electron occurs from the core atomic state to a final unoccupied state that is the relaxed excited state in the presence of the core hole at the 1s level screened by other electrons. In the dipole approximation, $\Delta l = \pm 1$ (l is the orbital momentum of the electron), the final state of the electron should have p character. Therefore, the pre-edge peak A can be attributed to the dipole-allowed transitions $|1s3d^{8+i}\underline{L}^i\rangle \rightarrow |\underline{1s}3d^{8+i}\underline{L}^{i-1}\rangle$, $i = 1, 2$ ($\underline{1s}$ denotes a Ni 1s core hole), to the final state (FS):

$$\Psi_{FS} = b_1|\underline{1s}3d^9L\rangle + b_2|\underline{1s}3d^{10}\underline{L}\rangle. \tag{7}$$

In the sudden approximation, the intensity of the pre-edge peak A is given by $|a_1b_1 + a_2b_2|^2$ [32]. One should note that both the ground Ψ_{GS} and final Ψ_{FS} states in NiO are characterized by a strong mixing of the oxygen 2p and nickel 3d orbitals.

Such an interpretation of the origin of the pre-edge peak A is strongly supported by self-consistent-field (SCF) multiple-scattering (MS) calculations performed recently for the Ni K edge for $La_{1-x}Nd_xNiO_3$ and $LaNi_{1-x}Fe_xO_3$ perovskites [34]. In these materials, nickel ions have the valence state 3+, and therefore their ground-state configuration consists of the four states $|3d^7\rangle$, $|3d^8\underline{L}\rangle$, $|3d^9\underline{L}^2\rangle$, and $|3d^{10}\underline{L}^3\rangle$. Among these, the latter three states are dipole allowed for the transition of the 1s(Ni) electron. In [34], only two configurations, $|3d^7\rangle$ and $|3d^8\underline{L}\rangle$, were taken into account in the calculations. The results obtained show that the intensity of the pre-edge peak A correlates strongly with the proportion of the $|3d^8\underline{L}\rangle$ configuration in the ground state [34]. Thus, we conclude that at the Ni K edge in c-NiO and the thin films, the proportions of the $|3d^{8+i}\underline{L}^i\rangle$, $i = 1, 2$, configurations in the ground state should be responsible for the intensity of the pre-edge peak A (figure 1(b)). Another possible interpretation of the pre-edge peak may be the 1s(Ni) $\rightarrow$ 3d(Ni) quadrupole transition; however, its intensity is expected [35] to be very low compared to that of the dipole transition 1s(Ni) $\rightarrow |3d^{8+i}\underline{L}^i\rangle$.

Note also that the effect of the thin-film non-stoichiometry, which is manifested as the presence of Ni^{3+} ions [2, 4], on the pre-edge intensity seems to be small in our case. In both charge-transfer and quadrupole-transition models, the presence of Ni^{3+} ions should lead to the increase of the pre-edge intensity (in the first model, due to an increase in the charge transfer from oxygens to more positively charged Ni^{3+} ions, but in the second model, due to an increase in the number of 3d(Ni^{3+}) empty states). However, experiment shows that the intensity of the pre-edge peak decreases on going from c-NiO to the thin films (figure 1).

As can be expected, the quantities a_i ($i = 0, 1, 2$) in (6) correlate with the value of the charge-transfer energy Δ (see table II in [29]), and, like Δ, are also related to the value of the pd-orbital mixing λ_{pd} and to the covalency of the nickel–oxygen bonding [33]. These correlations are well illustrated by the following two examples. Note that since in the interpretation of the K-edge absorption we are interested in states with one or more holes at the ligand sites, from here on only the quantities a_1 and a_2 will be discussed.

The first example is a series of nickel dihalides (NiI_2, $NiBr_2$, $NiCl_2$, NiF_2) and nickel oxide [29], for which it was clearly shown that a_1 and a_2 correlate strongly with the ligand electronegativity X_a [36]. In particular, it was found (see table II in [29]) that a_1 decreases from 0.44 for NiI_2 ($X_I = 2.5$) to 0.32 for $NiBr_2$ ($X_{Br} = 2.8$), 0.23 for $NiCl_2$ ($X_{Cl} = 3.0$),

0.21 for NiO ($X_O = 3.5$), and ∼0 for NiF_2 ($X_F = 4.0$), which is the most ionic compound. The value of a_2 is substantially smaller than a_1, but it also decreases (see table II in [29]) from 0.09 for NiI_2 to 0.07 for $NiBr_2$, 0.06 for $NiCl_2$, 0.06 for NiO, and ∼0 for NiF_2. Thus, for compounds in which the nickel ions have the valence state 2+, the $a_1 \equiv |3d^9\underline{L}\rangle$ ground-state configuration is mainly responsible for the intensity of the pre-edge peak.

The second example, represented by the $La_{2-x}Sr_xNiO_4$ system [37], is more complicated. $La_{2-x}Sr_xNiO_4$ is an analogue of the high-T_c Cu–O-based superconductors [38]; the Sr-induced hole population results in metallic behaviour beyond $x \approx 0.8$ [39]. The intensity of the pre-edge peak A for $La_{2-x}Sr_xNiO_4$ ($0 \leqslant x \leqslant 1.3$) increases uniformly upon Sr doping, and is about three times larger at $x = 1.3$ than for the undoped material ($x = 0$) [37]. The origin of the peak A was interpreted in [37] as being due to the 1s(Ni) → 3d(Ni) quadrupole transition, and an increase of its intensity was related to an increase in Ni p/Ni d hybridization, which opens up a dipole-allowed transition channel [37]. However, in the light of the results obtained in [29, 34, 38, 40], a more likely interpretation is as follows. Doping by strontium leads to the increase of the formal valence state of nickel ions from 2+ (at $x = 0$) to 3+ (at $x = 1$) and 4+ (at $x = 2$) that results in an increase of the charge transfer from oxygen to nickel ions, and, thus, in an increase of the proportion of the $|3d^{8+i-x}\underline{L}^i\rangle$ ($i = 1, \ldots, 2 + x$) ground-state configurations with holes present in the oxygen-derived band. These configurations support the dipole-allowed excitations of the Ni 1s core electron, so they can be readily observed in the Ni K-edge absorption spectra of $La_{2-x}Sr_xNiO_4$ as a pre-edge feature whose intensity increases with x. Such an interpretation accords well with (i) the insulator-to-metal (IM) transition [39], observed in $La_{2-x}Sr_xNiO_4$ at $x \approx 0.8$ upon doping with strontium, and (ii) the accompanying decrease of the distortion of the NiO_6 octahedra (the NiO_6 octahedron is less distorted in the metallic phase) [37], which are the 'fingerprints' of the measure of the nickel–oxygen bond covalency being in correlation with the variation of the intensity of peak A. According to the ZSA picture [19], the IM transition in $La_{2-x}Sr_xNiO_4$ may be viewed as a transition from a charge-transfer insulator to a semi-metal state in which the bandwidths of the occupied oxygen 2p valence band and the unoccupied nickel 3d conduction band increase. As the bandwidths grow, the nickel–oxygen pd covalent mixing, λ_{pd}, also becomes larger [41]. The latter means an increase in the proportion of $|3d^{8+i-x}\underline{L}^i\rangle$ ($i > 0$) ground-state configurations, leading to an increase of the pre-edge peak intensity. This explanation coincides well with the ones for nickel dihalides and nickel oxide [29].

The above examples show that a decrease of the nickel–oxygen bond covalency correlates strongly with the proportion of ground-state configurations with hole(s) in the oxygen 2p states. Since it is supposed that these configurations are responsible for the intensity of the pre-edge peak A [34], then, coming back to NiO_x thin films, one can conclude that a reduction of the intensity of peak A in the thin films (figure 1(b)) indicates an increase of the ionicity of the nickel–oxygen bonding [42]. If this conclusion is correct, then, in the thin films, the oxygen and nickel orbitals should become less mixed and more spatially localized in the vicinity of the cores. Since crystalline c-NiO is a type-II antiferromagnet with the Néel temperature $T_N = 523$ K [43], the decrease of the degree of covalent mixing λ_{pd} should lead to a reduction of the strength of the 180°, 90°, and Ni–O–Ni interactions, and, thus, to a decrease of the magnitude of T_N. Within the mean-field theory, the transition temperature of the Ising model is [44] $T_N = 2z|J|S(S+1)/3k_B$, where S is the total spin moment, k_B is the Boltzmann constant, z is the number of second-nearest-neighbour metal ions involved in the superexchange interaction, and J is the antiferromagnetic coupling constant, $J \equiv J_{cac}(180°) \propto \lambda_{pd}^4$ [41], $\propto 1/\Delta^3$ [19]. Therefore, there are two parameters that modify the T_N-value. The first parameter is z, and its influence, assuming J = constant,

on $Ni_cMg_{1-c}O$ solid solutions was studied recently [45, 46]. The second parameter is J, and its effect depends strongly on the change of the covalent mixing parameter λ_{pd} [41] or the charge-transfer energy Δ [19]. Thus, it is expected that an increase of Δ, estimated from the decrease of the pre-edge peak intensity, should affect the magnetic properties of NiO thin films, leading to the lower value of the Néel temperature T_N for the films with smaller grain size. The influence of the crystal grain size on the magnetic properties of NiO was studied in [47, 48]. It was observed [47, 48] that particles of nickel oxide less than 100 nm in size show superparamagnetism that becomes stronger as the crystallite size decreases, although no change in the Néel temperature T_N occurs. Nevertheless, a change in T_N was observed recently for an epitaxially grown 20-monolayer NiO film [49], where the Néel temperature ($T_N = 470$ K) was found to be lower than that of the bulk nickel oxide ($T_N = 523$ K [43]).

The change in the nickel–oxygen bonding in NiO_x thin films, determined from a variation of the pre-edge peak intensity in figure 1, should lead to a modification of the interatomic interactions. Therefore, one expects a relaxation of the crystal lattice to a new stable/metastable state which is closer to the original one when there is less change in the Ni–O bonding. This expectation accords well with the results of the EXAFS analysis (see section 3.2), which will be discussed below.

A comparison of the values of the area-weighted average grain sizes $\langle D \rangle_{area}$ (table 2), obtained within the RGB model [20], allows us to conclude that NiO_x thin films have nanocrystalline structure, with the average grain size being smaller in films deposited with lower oxygen contents in the $Ar–O_2$ sputter atmosphere. Also, since the value of t (table 2) is close to zero, most of the ions are located at crystal lattice sites, and, thus, the thin-film structure can be well described by the non-reconstructed grain-boundary model [20]. However, in contrast to the case of nanocrystalline pure metals (see [20] and references therein), the crystal lattice of the intragrain regions in NiO_x thin films seems to be distorted, which is reflected in the values of the coordination shell radii and the EXAFS MSRDs (table 1).

In thin films, a shortening by $\sim$0.02 Å, compared to that for c-NiO, of the average distance between the nickel ions and oxygens, situated in the first coordination shell, is observed, whereas the interatomic spacings from the outer shells, where nickel ions dominate in the formation of the EXAFS signals, increase progressively (table 1). The latter dependence (figure 5(b)) was used to estimate the intragrain lattice parameter a in the thin films: it was found to be equal to 4.20 Å and 4.21 Å for films No 1 and No 2, respectively. These values are in good agreement with the one determined by means of XRD [15]: $a_{XRD} = 4.22$ Å. One should note that an increase of the distance between nearest-neighbour Ni ions similar to that found in the present work was also observed for small (about ten Ni atoms) nickel oxide clusters enclosed in *Y*-zeolite [51].

Besides the variation of the interatomic spacings, an increase of the disorder, probed by means of the EXAFS MSRD σ^2, was observed in the thin films (table 1). Note that the MSRD values relative to those of c-NiO are larger for thin film No 2, which was deposited with a smaller oxygen content in the sputter atmosphere. It is interesting to compare the MSRD values for the first two coordination shells in the thin films (table 1), and in c-NiO and $Ni_cMg_{1-c}O$ solid solutions (see table 1 in [21]). The room temperature values of σ^2 for c-NiO are equal to 0.0038 Å^2 and 0.0054 Å^2 [21] for the first and second shells, respectively. Since the rock-salt crystal structure of c-NiO is perfect with good precision [50], these values can be considered as being just due to the thermal vibrations whose amplitude is related to the strength of the Ni–O chemical bonding and of the magnetic Ni–O–Ni superexchange interactions. In the rock-salt structure, formed by close packing

of anions, the metal ions are primary candidates for participating in possible displacements. This situation occurs in $Ni_cMg_{1-c}O$ solid solutions, where nickel ions shift upon dilution (with decreasing c) to the off-centre positions [21]. Such displacements lead upon dilution to the increase of the average Ni–O distance in the first shell by $\sim$0.017 Å, while the average Ni–Ni distance in the second shell remains nearly unchanged [21]. Besides this, the MSRD values for both Ni–O and Ni–Ni atom pairs decrease upon dilution, by 26% and 56%, respectively, suggesting the strengthening of Ni–O and Ni–Ni interactions, presumably due to the so-called 90° exchange [21].

In contrast to the case for $Ni_cMg_{1-c}O$ solid solutions, the disorder in NiO_x thin films, probed by means of the EXAFS MSRD σ^2 (table 1), increases by about 132% and 158% in the first shell and by about 56% and 93% in the second shell (the first number is for sample No 1 and the second number to sample No 2). Also, in the outer shells, where the contribution of nickel atoms dominates, the MSRD values are larger for the thin films than for c-NiO (see table 1 and figure 5(c)). Such variation of the MSRDs is too large to be explained by just the change of the amplitude of the thermal vibrations—in particular, because the relative displacements of the ions in the outer shells are uncorrelated, so the thermal MSRD should 'saturate' for distant atoms. However, this is not the case for the thin films (figure 5(c)). Also the nanocrystalline nature of the thin films affects only the coordination numbers, and not the MSRDs [20]. Therefore, we attribute some of the increase of the MSRDs for the thin films to an increase in static disorder corresponding to displacements of all of the ions from their positions in the perfect c-NiO lattice. This result is consistent with the conclusion, deduced above from the XANES analysis, that in thin films, a relaxation of the intragrain crystal lattice occurs to a new stable/metastable state due to the change in the nickel–oxygen bonding.

5. Summary and conclusions

In summary, we have presented a Ni K-edge x-ray absorption spectroscopy study of nickel oxide, NiO_x, thin films, prepared by reactive dc magnetron sputtering of a nickel target in an atmosphere that is an $Ar–O_2$ mixture.

The structural parameters, obtained from the EXAFS analysis, are compared to those of crystalline c-NiO and $Ni_cMg_{1-c}O$ solid solutions [21]. Application of a recently developed model [20] of nanocrystalline solids to our results shows that NiO_x thin films have nanocrystalline structure, with a non-reconstructed grain-boundary region. The average grain sizes are estimated from the ratio of the coordination numbers for the thin films and the crystalline c-NiO according to [20]; they are equal to 21 ± 3 Å and 34 ± 5 Å for the thin films deposited in the sputter atmospheres with the oxygen contents 30% and 100%, respectively. Thus, the grain size becomes smaller with the decrease of the oxygen content in the sputter atmosphere.

Besides the reduction in the number of atomic neighbours in the crystal lattice coordination shells beyond the first one, an increase in the structural disorder relative to that in c-NiO by $\Delta\sigma^2 \approx 0.003$–$0.009$ Å^2 and of the intragrain lattice parameter by $\Delta a \approx 0.016$–0.034 Å is observed for the thin films. These changes are attributed to a relaxation of the crystal lattice in the intragrain region to a new stable/metastable state. The reason for such relaxation is the change in the character of the nickel–oxygen interactions causing the Ni–O bonding to become more ionic. This conclusion is supported by a variation of the intensity of the pre-edge peak, corresponding to the dipole-allowed transitions $|1s3d^{8+i}\underline{L}^i\rangle \rightarrow |\underline{1s}3d^{8+i}\underline{L}^{i-1}\rangle$, $i = 1, 2$ ($\underline{L}$ denotes an O 2p hole and $\underline{1s}$ stands for a Ni 1s core hole). The experiment shows that the intensity of the pre-edge peak is smaller for

thin films than for c-NiO. This fact is interpreted within the Zaanen–Sawatzky–Allen model [19] as being due to an increase of the oxygen–nickel charge-transfer energy Δ, which is accompanied by a lowering of the proportion of the $3d^{8+i}\underline{L}^{i}$, $i = 1, 2$, ground-state configurations, and by an increase in the ionicity of the Ni–O bonds.

Acknowledgments

JP and AK are grateful to Professor E Burattini and the staff of the PWA laboratory of the ADONE storage ring for providing the beam time and support during the measurements. This work was supported in part by the International Science Foundation, Grants No LF8000 and LJ8100.

References

[1] Svensson J S E M and Granqvist C G 1986 *Appl. Phys. Lett.* **49** 1566
[2] Sato H, Minami T, Takata S and Yamada T 1993 *Thin Solid Films* **236** 27
[3] Granqvist C G 1995 *Handbook on Inorganic Electrochromic Materials* (Amsterdam: Elsevier Science)
[4] Yamada S, Yoshioka T, Miyashita M and Urabe K 1988 *J. Appl. Phys.* **63** 2116
[5] Antolini E 1992 *J. Mater. Sci.* **27** 3335
[6] Austin I G, Clay B D, Turner C E and Springthorpe A J 1968 *Solid State Commun.* **6** 53
Austin I G and Mott N F 1969 *Adv. Phys.* **18** 41
Iguchi E and Akashi K 1992 *J. Phys. Soc. Japan* **61** 3385
Iguchi E, Lee K J and Iguchi A 1993 *J. Phys. Soc. Japan* **62** 1135
[7] Nilsson T M J and Niklasson G A 1990 *Proc. SPIE* **1272** 129
[8] Rechtin M D and Averbach B L 1975 *J. Phys. Chem. Solids* **36** 893
[9] Estrada W, Andersson A M and Granqvist C G 1988 *J. Appl. Phys.* **64** 3678
[10] Wruck D A and Rubin M 1993 *J. Electrochem. Soc.* **140** 1097
[11] Liberman M L and Medrud R C 1969 *J. Electrochem. Soc.* **116** 242
[12] Willems H, Kobussen A G C, Vinke I C, de Wit J H W and Broers G H J 1985 *J. Electroanal. Chem.* **194** 287
[13] Miedzinska K M E, Hollebone B R and Cook J G 1988 *J. Phys. Chem. Solids* **49** 1355
[14] Yamada S, Yoshioka T, Miyashita M and Urabe K 1988 *Proc. SPIE* **1016** 34
[15] Andersson A M, Estrada W, Granqvist C G, Gorenstein A and Decker F 1990 *Proc. SPIE* **1272** 96
[16] Bets V, Zamozdiks T, Lusis A, Purans J, Bausk N and Sheromov M 1987 *Nucl. Instrum. Methods Phys. Res.* A **261** 173
[17] Burattini E, Purans J and Kuzmin A 1993 *Japan. J. Appl. Phys. Suppl.* 2 **32** 655
[18] Babulanam S M, Estrada W, Hakim M O, Yatsuya S, Andersson A M, Stevens J R, Svensson J S E M and Granqvist C G 1987 *Proc. SPIE* **823** 64
[19] Zaanen J, Sawatzky G A and Allen J W 1985 *Phys. Rev. Lett.* **55** 418
Zaanen J and Sawatzky G A 1987 *Can. J. Phys.* **65** 1262
[20] Löffer J and Weissmüller J 1995 *Phys. Rev.* B **52** 7076
[21] Kuzmin A, Mironova N, Purans J and Rodionov A 1995 *J. Phys.: Condens. Matter* **7** 9357
Mironova N, Kuzmin A, Purans J and Rodionov A 1995 *Proc. SPIE* **2706** 168
[22] Kuzmin A 1995 *Physica* B **208+209** 175
Kuzmin A 1996 *EDA: EXAFS Data Analysis Software Package; User's Manual* (available from the author)
Kuzmin A 1997 *J. Physique* IV at press
[23] Stern E A and Heald S M 1983 *Handbook of Synchrotron Radiation* ed E E Koch (New York: North-Holland) ch 10
[24] Kizler P 1992 *Phys. Rev.* B **46** 10 540
[25] Teo B K 1986 *EXAFS: Basic Principles and Data Analysis* (Berlin: Springer)
[26] Stern E A 1993 *Phys. Rev.* B **48** 9825
[27] Haubold T, Birringer R, Lengeler B and Gleiter H 1989 *Phys. Lett.* **135A** 461
[28] Hermann H 1991 *Mater. Sci. Forum* **78** 1
[29] van der Laan G, Zaanen J, Sawatzky G A, Karnatak R and Esteva J M 1986 *Phys. Rev.* B **33** 4253
van Veenendaal M A and Sawatzky G A 1994 *Phys. Rev.* B **50** 11 326

[30] van der Laan G, Westra C, Haas C and Sawatzky G A 1981 *Phys. Rev.* B **23** 4369
[31] Fujimori A and Minami F 1984 *Phys. Rev.* B **30** 957
Fujimori A, Minami F and Sugano S 1984 *Phys. Rev.* B **29** 5225
[32] Mizokawa T, Fujimori A, Arima T, Tokura Y, Mori N and Akimitsu J 1995 *Phys. Rev.* B **52** 13 865
[33] Bocquet A E, Mizokawa T, Fujimori A, Matoba M and Anzai S 1995 *Phys. Rev.* B **52** 13 838
[34] García J, Blasco J, Proietti M G and Benfatto M 1995 *Phys. Rev.* B **52** 15 823
[35] Bersuker I B 1976 *Electronic Structure and Properties of Coordination Compounds* (Leningrad: Khimia)
[36] Pauling L 1960 *The Nature of the Chemical Bond* (Ithaca, NY: Cornell University Press)
[37] Sahiner A, Croft M, Guha S, Perez I, Zhang Z, Greenblatt M, Metcalf P A, Jahns H and Liang G 1995 *Phys. Rev.* B **51** 5879
[38] Bednorz J G and Müller K A 1988 *Rev. Mod. Phys.* **60** 585
[39] Kuiper P, Van Elp J, Sawatzky G A, Fujimori A, Hosoya S and de Leeuw D M 1991 *Phys. Rev.* B **44** 4570
[40] Fujimori A, Takayama-Muromachi E, Uchida Y and Okai B 1987 *Phys. Rev.* B **35** 8814
[41] Goodenough J B 1971 *Prog. Solid State Chem.* **5** 145
[42] Kuzmin A, Mironova N and Purans J 1997 *J. Phys.: Condens. Matter* **9** 5277
[43] Roth W L 1958 *Phys. Rev.* **110** 1333
[44] van Vleck J H 1941 *J. Chem. Phys.* **9** 85
[45] Menshikov A Z, Dorofeev Yu A, Klimenko A G and Mironova N A 1991 *Phys. Status Solidi* b **164** 275
Menshikov A Z, Dorofeev Yu A, Klimenko A G and Mironova N A 1990 *Pis. Zh. Eksp. Teor. Fiz.* **51** 640
[46] Feng Z and Seehra M S 1992 *Phys. Rev.* B **45** 2184
[47] Richardson J T and Milligan W O 1956 *Phys. Rev.* **102** 1289
[48] Richardson J T, Yiagas D I, Turk B and Forster K 1991 *J. Appl. Phys.* **70** 6977
[49] Alders D, Vogel J, Levelut C, Peacor S D, Hibma T, Sacchi M, Tjeng L H, Chen C T, van der Laan G, Thole B T and Sawatzky G A 1995 *Europhys. Lett.* **32** 259
[50] Massarotti V, Capsoni D and Berbenni V 1991 *Z. Naturf.* a **46** 503
[51] Matsuo A, Satou S, Suzuki M, Sano M and Nakano H 1991 *Z. Phys.* D **18** 281